Permeability measurement of a 3D-printed AlSi10Mg porous medium: comparisons between first results with different experimental and numerical techniques

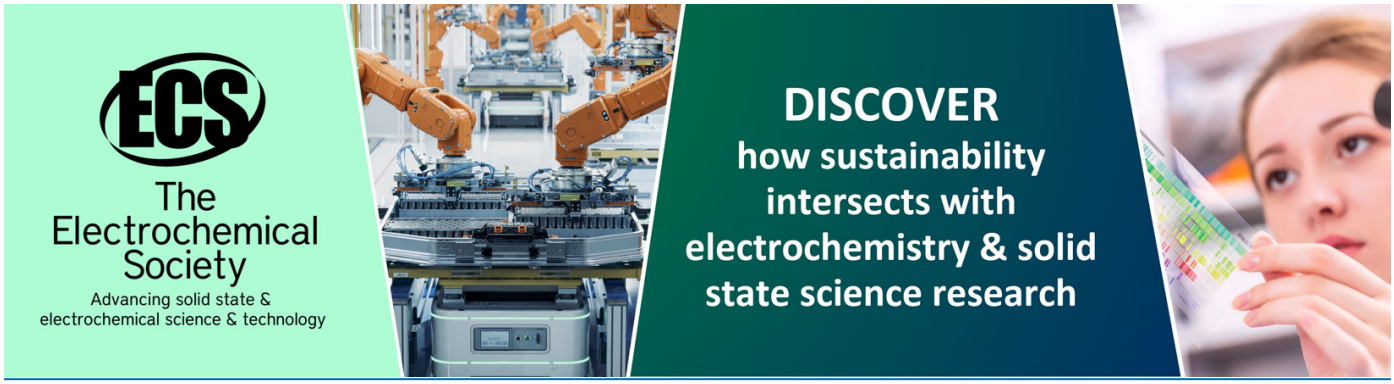

Permeability measurement of a 3D-printed AlSi10Mg porous medium: comparisons between first results with different experimental and numerical techniques

L Vitali[1], G Brambati[2], R Caruana[1], S Foletti[2], M Guilizzoni[1] and A Niro[1]*

[1] Department of Energy, Politecnico di Milano, Via Lambruschini 4, 20156 Milan, Italy
[2] Department of Mechanical Engineering, Politecnico di Milano, Via La Masa 1, 20156 Milan, Italy
* Corresponding author: alfonso.niro@polimi.it

Abstract. In this work, the permeability of a 3D-printed, AlSi10Mg porous medium, with porosity ε = 0.3 and an effective pore radius of 48 μm, developed to operate as wick in a sinter-like heat pipe, has been investigated by means of two different experimental approaches, and of two different numerical methods. The two experimental methods are the capillary rise tests, from which permeability was estimated by fitting the theoretical capillary rise curve to the experimental data, and the direct measurement of the the mass flow rate across the porous sample at an imposed pressure difference. The numerical simulations were performed too using two different approaches and software tools, namely, Lattice-Boltzmann with Palabos, and Finite-Volumes with OpenFOAM. In both cases, the simulation domain was reconstructed from a micro-computer aided tomographic scan of a porous medium sample. Preliminary simulations were run on a simple configuration, both to check simulation setup and validate results, and mesh independence was assessed. Then, pressure-driven and velocity-driven simulations of an incompressible fluid flow across the domain were performed, from which the permeability was estimated using Darcy and Darcy-Forchheimer equations. The results show that the methods, while not in complete agreement, provide a useful estimate. The numerical methods also complement the information given by the experimental techniques by highlighting the flow paths, and allow to analyze scenarios of increased and decreased porosity.

1. Introduction

Metallic porous media are of interest in a wide range of engineering fields, as chemical [1], biomedical [2], and heat transfer [3,4]. Many fabrication techniques are used for this type of media, including sol-gel, polymer porosifier method, foaming method, and additive manufacturing (AM) [5]. In particular, additive manufacturing, also known as 3D-printing, have become increasingly used in recent years, as it gives the possibility to manufacture embedded components in structures.

A common application of porous media in heat transfer field is using them as wick for heat pipes [6], as their structure promotes the capillary rise of the liquid, thus allowing the device operation also against gravity. Heat pipe performances are strongly influenced by the wick material, which must be compatible with the working fluid [7] and the structure, and it must adequately satisfy the need of a trade-off between the requirements of high capillary pressure and high permeability [8]. The first one can be

estimated based on the pore radii and the contact angle. The latter, quantifying the medium's resistance to fluid flow, can be measured or estimated in several ways.

One experimental way to measure permeability of a porous media is to perform a capillary rise test. This method has been used by both Zhang et al. [9] and Deng et al. [10] to characterize the performance of sintered copper wicks, for cylindrical heat pipes, and sintered nickel and copper wicks for loop heat pipes, respectively. Furthermore, Darcy's law [11] can be used to estimate the permeability value of a porous medium by directly measuring the mass flow rate across the sample, and consequently the flow velocity, at imposed pressure difference [12].

Another possibility for estimating permeability of porous media is performing numerical simulations. This has been done by Eshghinejadfard et al. [13], who used the Lattice Boltzmann method with either single or multiple relaxation time to calculate the permeability of three-dimensional hydrodynamics porous media at low Reynold numbers, as well as by Narváez et al. [14], who used the Lattice Boltzmann method as well, but focusing on the choice of the simulation set-up parameters, and on their influence on the final results. Moreover, Jeon and Byon [15] used CFD to estimate the permeability of a dual-height micro-post wick while considering the meniscus shape. The domain for the CFD simulations can be reconstructed from micro-computer aided tomography scans of real samples, as for example in the work by Otaru and Samuel [16], in which the reader can also find additional references to significant papers about this topic.

This work aims at estimating the permeability of a 3D-printed aluminum porous medium, developed to be used as wick in a sintered-like heat pipe, using both experimental and numerical methods. More specifically, two experimental techniques, namely the capillary rise test and the direct measurement of mass flow rate at different pressure differences, and two numerical methods, namely Lattice Boltzmann and Finite Volume, have been investigated and the results are compared and discussed.

2. Experimental setups and results

2.1. Samples

The additive-manufactured-samples have been made by Beam-IT S.p.A in different printing sessions. In order to produce a sinter-like porous structure, also referred to as "wick" in this paper, several preliminary trials were necessary to find a combination of printing parameters which allows to form a mechanically-resistant aggregate of the AlSi10Mg powder with a significant porosity. Such parameters are summarized in table 1. The measurements presented below use a 10-cm-high half-pipe sample, with a 4 mm wick thickness, and printing direction orthogonal to the sample's vertical axis for the capillary rise test, and a 2-cm-long cylinder with a 1 cm diameter wick, externally filleted to be attached to a 1/2" pipe fitting, for the direct mass flow rate measurement. The μCT section used for the numerical models, described in Section 3.1, has been retrieved from a 15-cm-long heat pipe sample, with a 1.6 cm internal diameter and a wick thickness of 2.4 mm. All these samples have been printed using the same parameters, however the geometrical differences between samples resulted in different porosity values, which are 0.30 and 0.26 for the capillary rise and the permeability samples, respectively. The tomographed section's porosity is dependent on the choice of a threshold parameter, which has been chosen to set a porosity value of 0.36. Figure 1 shows the heat pipe section and the samples used for the permeability tests, as visual reference.

Table 1. Porous medium printing parameters

Print parameter	Unit	Value	Print parameter	Unit	Value
Layer thickness	μm	60	Speed	mm/s	2350
Hatch Distance	μm	140	Energy	J/mm^3	10.13
Power	W	200	Focal / spot size	μm	160

(a) (b)

Figure 1. Tomographed heat pipe section with highlight of the wick portion used for computational analyses (a) and samples for the direct measurement permeability test (b).

2.2. Capillary rise test

The capillary maximum rise and the capillary rate-of-rise tests can be used to characterize the capillary performance parameter of a wick structure. At any time, capillary pressure ΔP_c is supposed in equilibrium with hydrostatic head ΔP_h, and friction pressure drop ΔP_f,

$$\Delta P_c = \Delta P_h + \Delta P_f \tag{1}$$

Assuming:

$$\Delta P_c = \frac{2\sigma\cos\theta}{r_p} \qquad \Delta P_h = \rho g h \qquad \Delta P_f = \frac{1}{K}\mu\varepsilon h\frac{dh}{dt} \tag{2}$$

where g is the gravity acceleration, h the liquid height, ε the porosity, σ the surface tension, ρ the mass density, μ the dynamic viscosity, θ the contact angle, r_p the average pore radius, and K the permeability. Substituting expressions 2 into equation 1 and, finally, solving the latter for the rise rate, the following equation is obtained:

$$\frac{dh}{dt} = \frac{2\sigma}{\mu\varepsilon}\frac{K\cos\theta}{r_p}\frac{1}{h} - \frac{\rho g K}{\mu\varepsilon} \tag{3}$$

As it can be seen from equation 3, the relation between time and the height reached by the liquid is a function of both the thermophysical and capillary properties of the used liquid, and the porous medium's properties, i.e. the pore radius r_p, the permeability K and the porosity ε. The porosity is measured by weighing the sample after being dried (4h at 50 °C in a ventilated oven), and after being saturated with ethanol, as described by Jafari et al. [17], hence the two unknowns are r_p and K. Assuming that all the properties are constant, numerical fitting of the experimental capillary rise trend *h(t)* can be performed to determine both. Different techniques can be used, as explained in detail by Elkholy et al. [18], and the outcome may vary depending on the method of choice. In this work the equation was numerically integrated using a forward finite difference approach, and the Matlab® function *fminsearch* – implementing a Nelder-Mead algorithm – was used to perform the fitting and to obtain the values of r_p and K that give the best agreement between the theoretical and experimental curves. This method has been found to provide more consistent results with respect to the other test methods for our experiments than the ones described in [18].

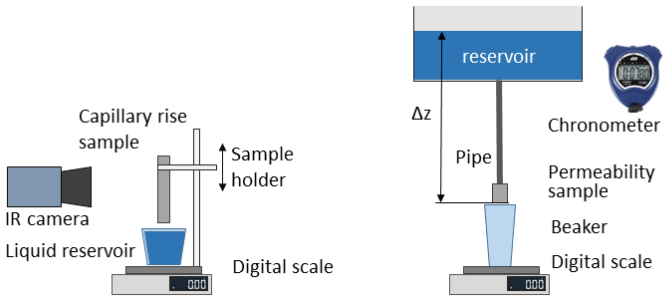

Figure 2. Capillary rise test set-up scheme (left) and permeability set-up scheme (right)

The capillary rise tests have been carried out with ethanol using simultaneously two different methods, for cross-validation. The first one consists of recording the capillary rise with a FLIR T450sc IR camera, for increased contrast between the wet and the dry surface, and considering the mass rise equal to the product of wetted height, sample cross-section, porosity, and fluid density. The second method consists of recording the mass decrease of ethanol contained in a liquid reservoir where, as showed in figure 2 (left), the tip of the sample is dipping. To achieve meaningful measurements, corrections have to be carried out to consider evaporation of ethanol both from the reservoir, as calibrated before the trial, and from the sample, considered proportional to the wetted height. The corrections are then applied, resulting in the curves shown in figure 3 (left). The comparison between the two complementary measurement techniques, i.e. balance and thermography, is also shown in figure 3 (left), where the saturation mass, i.e. the maximum mass of liquid that the porous material is able to absorb from dry conditions, is also evidenced. The main uncertainties associated with the two methods are due to the retrieval of the wet-dry interface for the IR camera data, and the corrections due to evaporation for the balance method. In this paper, solely the latter is used for the retrieval of the results. Figure 3 (right) shows the experimental mass rise curve and the finite difference solution of equation 3 using r_p and K resulting from the fitting procedure. Such values may vary with the total experiment time, i.e. the resulting values are 50, 43 and 40 μm for r_p and 3.7, 2.3 and 2.0 μm^2 for K, considering 500, 1000 and 1500 s of the rising curve.

2.3. Flow rate based measurement

As permeability measures the "resistance" of a fluid to flow through a material, usually it is measured by recording the mass flow rate m of a fluid with known properties while imposing a pressure difference ΔP across a sample long L.

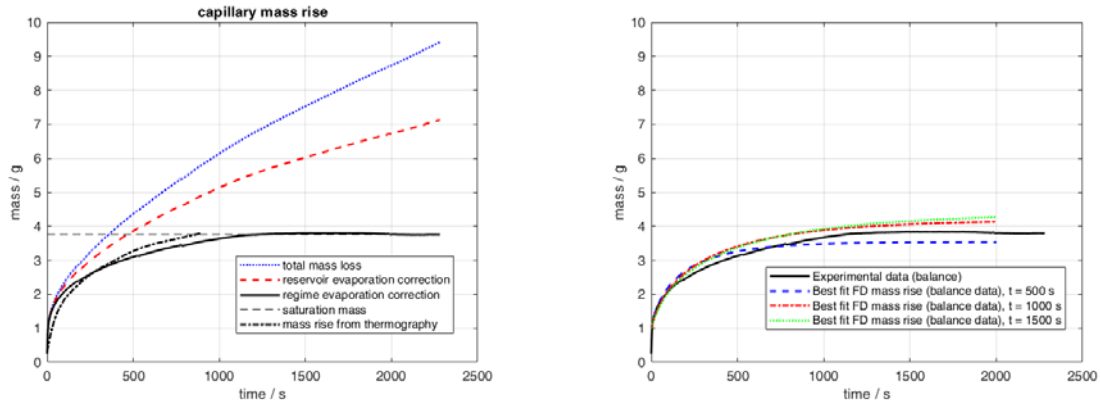

Figure 3. Measurement of the mass absorbed by the specimen before and after corrections for evaporation and comparison with thermographic data (left), comparison with a finite difference (FD) solution of equation 3 with r_p and K obtained from curve fitting

In general, a Darcyan permeability coefficient K_1 [m^2] and a Forchheimer term K_2 [m], which accounts for the pressure losses, can be introduced according to the following equation:

$$\frac{\Delta P}{L} = \frac{1}{K_1}\mu w + \frac{1}{K_2}\rho w^2 \quad (6)$$

However, when inertial effects are negligible, i.e. the flow velocity *w* is less than 0.1 m/s, as always verified in this work, only the first term of equation 6 is considered, and hence $K = K_1$.

The measurement of K is carried out by simply putting a reservoir of acetone, large enough so that its free surface does not significantly lower during the trial, at known heights Δz, namely 1.1, 1.5 and 1.9 m respectively, and by measuring the resulting steady-state mass flow rate across the sample. Equation 6 is then applied to retrieve K. A scheme of the experimental setup used is depicted in figure 2 (right) showing the sample and the reservoir connected by a 2-m-long pipe with an internal diameter of 1.6 mm. A corrective term ΔP_{loss} to take into account the friction loss across the pipe can be easily calculated with Poiseuille's equation for friction factor, as flow is laminar across the whole experimental range. The results of these experiments are reported in table 2, which shows that the permeability has a high degree of independency from ΔP, and the average value for the tested sample is 3.10 μm^2.

Table 2. Results of the direct permeability measurement experiment

H [m]	1.1	1.5	1.9
ΔP [Pa]	8294	11550	14728
$\Delta P - \Delta P_{loss}$ [Pa]	6904	9611	12262
m_{vol} [ml/s]	0.545	0.761	0.968
K [μm^2]	3.10	3.10	3.09

3. Numerical setups and results

3.1. Computational domain

The domain for the final simulations was created on the basis of a micro-computer-aided tomographic (μCT) scan of the same porous material used for the experimental test. The porous sample was scanned with a resolution of 10 μm and reconstructed. The reconstruction was segmented into solid and air regions according to a threshold which was selected to have a final porosity consistent with some independent porosity measurements. The selected porosity for the numerical simulations is 0.36, even though a sensitivity analysis is carried out with the Lattice-Boltzmann method as described in paragraph 3.3. From such segmentation an iso-surface, representing the solid boundaries, was extracted and exported as an STL file. To facilitate the setup of the boundary conditions and the post-processing to calculate the permeability, two thin regions were added at the beginning and at the end of the porous domain extracted from the μCT reconstruction. The bounding box of the domain has dimensions 1 mm × 1 mm × 4 mm and it is shown along with CFD results in figure 5.

3.2. Finite Volume simulations

The numerical simulations using the Finite Volume method were performed using the CFD toolbox OpenFOAM® [19]. For the present simulations, the steady-state, incompressible, simpleFoam solver was selected and preliminarily validated by simulating a single duct and an array of circular mini-channels, and comparing the pressure-drop results to the estimates of the analytical models. The mean absolute error (MAE) on the developed flow region along the single duct was 0.33 %, with a mean absolute deviation (MAD) equal to 0.13%. On the developed flow regions of the array of parallel mini-channels the MAE was 0.69% with a MAD of 0.46%. Mesh independence was assessed by using different meshes with and without mesh refinement near the walls for the porous medium. Meshes up to 4.5 million cells were tested, and the final used mesh consisted of 1.3 million cells. For all simulations, the fluid was acetone, whose values of density and viscosity were taken at 50 °C and 0.1 MPa,

namely, 756 kg/m^3 and 2.451×10^{-4} Pa·s, respectively. Simulations were performed for both velocity-driven case, with an inlet velocity of 0.1–5 mm/s, and pressure-driven case, for a 1 Pa pressure difference between inlet and outlet. Both types of simulations easily converged, with very stable values for the quantities of interest and residuals lower than 10^{-6}, in less than 1000 iterations. At all the investigated velocities, flow is laminar, so no turbulence models were used. For the wall of both porous medium and channels, a classic no-slip boundary condition was set. Steady-state simulations were performed using the SIMPLE algorithm.

Focusing the attention on the simulations on the porous medium, figure 5 shows an example of the results that were obtained, in terms of pressure distribution in the domain and velocity field and streamlines in a slice of the same.

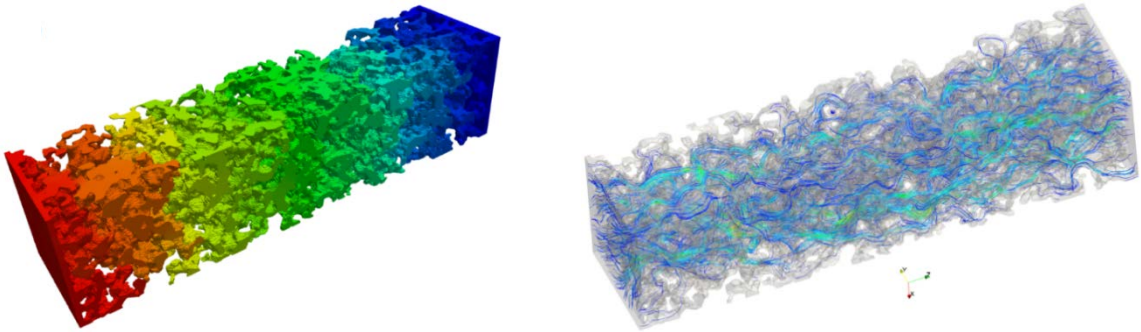

Figure 5. Examples of the finite volumes simulation results on the porous medium: pressure distribution (left) and flow streamlines (right) in the domain.

From the pressure differences, obtained in the velocity-driven simulations, or from the superficial velocity, obtained in the pressure-driven simulations, permeability was calculated with both the Darcy and the Darcy-Forchheimer approaches, i.e. by equation 6. As velocities are very low, as expected, the inertial term has a negligible influence and hence the two approaches returned practically identical values. With the Darcy approach the mean value of the calculated permeability is 11.8 μm^2, with a standard deviation of 0.06 m^2 when varying the superficial velocity; with the Darcy-Forchheimer approach – performing a quadratic fitting with zero intercept of the pressure drop as a function of the superficial velocity – the value is 11.9 μm^2, with a percentage difference between these two values of 1.4%.

3.3. Lattice-Boltzmann simulations

In this study, the open-source code Palabos (Parallel Lattice Boltzmann Solver) [21] was used to solve Lattice-Boltzmann equations. At the end of the simulation, the value of permeability can be calculated in accordance with Darcy's law, which is defined for a single-phase 1D fluid flow as follows:

$$K_{LB} = \nu_{LB} \frac{< u_{LB} >}{\Delta P_{LB}/L_{LB}} \tag{7}$$

where < u > is an averaged velocity of the fluid and ν the kinematic viscosity.. The subscript LB in equation 9 indicates that the quantities are expressed in lattice units, since Palabos operates entirely in not-dimensional units. Therefore, it is necessary to determine conversion coefficients to retrieve the physical meaning of the results. The spatial unit conversion coefficient Δx is readily available as it corresponds to the voxel size used in the CT-scans, whereas the temporal unit coefficient Δt can be determined by combining the physical value of the fluid's kinematic viscosity with Δx. To impose a pressure difference ΔP as a boundary condition, the physical pressure difference must first be divided by the fluid density to obtain a value expressed solely in terms of length and time. Subsequently, Δx and

Δt are used to calculate the pressure difference in lattice units. In regard to permeability, the physical value can be obtained by multiplying the simulation result by $(\Delta x)^2$, whereas the physical velocities multiplying the simulation results by the Δx-to-Δt ratio. Pressure-independency and validation tests have been again conducted on capillary bundles composed by straight tubes, before applying the method to the wick and a slight overprediction of the permeability, circa 6%, has been observed with respect to analytical pressure-drop solutions.

Multiple simulations were performed with varying pressure differences in order to verify the pressure-independence of the permeability value obtained. Throughout the simulation, the average energy standard deviation was monitored, and convergence was considered achieved when its value fell below the threshold of 10^{-8}. The computed permeability for the analysed porous sample was 16.3 μm^2. Figure 6 (left) shows a visualization of the velocity field. Additional porous samples were also extracted from the CT-scan of the wick to investigate the influence of varying porosity on permeability. The results of this study are depicted in figure 6 (right).

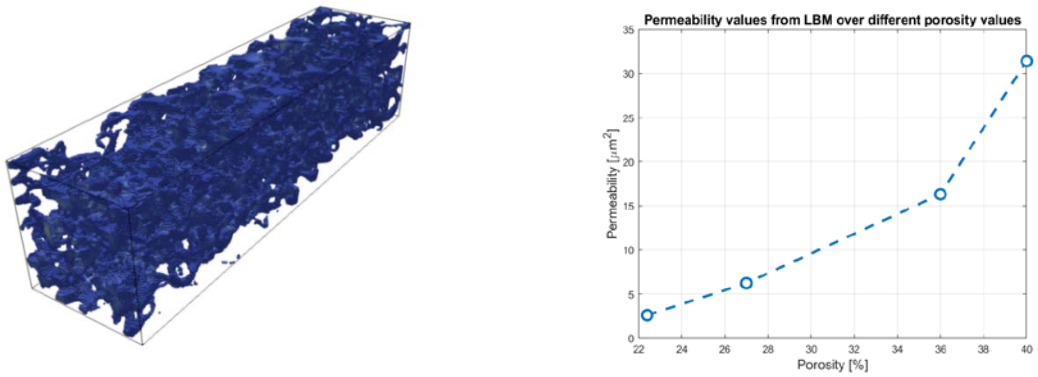

Figure 6. Fluid field visualization from LBM simulations (left) and permeability values for samples with different porosity (right)

4. Discussion and conclusions

Two experimental and two numerical methods have been applied to estimate the permeability of additively-manufactured porous media, in the context of evaluating a wick structure for heat pipes. The considered samples, and one virtual reconstructions by μCT, are characterized by different porosities due to the different geometry of the samples, which in turn causes different resulting structures, even for the same printing parameters. Furthermore, the selection of a threshold value for the computerized geometry may significantly vary the porosity, hence the permeability of the sample. A recap of the results is presented in table 3.

Table 3. Permeability results for different measurement / estimation methods

Porosity	K [μm²]	Method
0.22	2.7	Numerical, lattice-Boltzmann
0.26	3.1	Experimental, mass flow rate measurement
0.27	6.0	Numerical, lattice-Boltzmann
0.29	2.0-3.7	Experimental, capillary rise
0.36	11.8	Numerical, finite volumes
0.36	16.3	Numerical, lattice-Boltzmann
0.40	32.0	Numerical, lattice-Boltzmann

As a general note, the estimation of *K* by measuring the mass flow rate shows good internal consistency with variations of imposed pressures, while the capillary rise test, due to the high evaporation rates of ethanol with respect to the measured data, needs either a controlled environment or a precise model of such phenomenon to retrieve qualitative data, but at the moment provides a

reasonable estimate for the purpose of evaluating the thermal models of heat pipes. The experimental data confirm the range of permeabilities measured by Gotoh et al. [22]. Finally, it should be pointed out that water cannot be employed in this test due to the low wettability of the aluminium porous structure.

Concerning the numerical methods, the lattice-Boltzmann method provides a value of K 40% higher than the finite volumes simulation, a difference which is higher than the 6% variation with respect to analytical solutions in simple test cases showed by the method's validation. The finite volume method performs well against validation cases, and should be the method of choice for any preliminary test based on design only, especially on porous media consisting of lattice structures, with production outcomes similar to the design. It should be pointed out that the used computational domain, while having its smaller side 20 times larger than the average estimated pore size, could not be statistically representative of the entire sample. For random porous media as the sinter-like structure presented in this paper, consistency issues between specimens, print direction and sample shape may arise, especially when confronting measurement techniques with different samples, however, the estimates obtained with the presented techniques are often accurate enough to evaluate the range of operating limits of the components in which they are used.

References

[1] Heydari A and Peyvandi K. 2019 *J. of Pet. Sci. and Eng.* **181**, 106235.
[2] Khanafer K and Vafai K. 2006 *Heat and Mass Trans.*, **42** 10, 939-53.
[3] Wang C Y and Cheng P 1997 *Adv. in heat trans.* **30** 93-196
[4] Badruddin I A, Khan, T Y and Baig M A A 2020 *Materials Today: Proceedings*, **24,** 1318-21.
[5] Zhao B, Gain A K, Ding W, Zhang L, Li X, and Fu, Y 2018 *Int. J of Adv. Manufacturing Tech.* **95**, 2641-2659.
[6] Iverson B D, Davis T W, Garimella S V, North M T, and Kang S S 2007 *J. of Thermophy. and Heat Trans.* **21**(2), 392-404.
[7] Caruana R, Gallazzi L, Iazurlo R, Marcovati M and Guilizzoni M 2022 *Fluids*, **7**(3), 109.
[8] Mwaba M G, Huang X, and Gu J 2006 *Int. J. of en. res.* **30** 7, 489-499.
[9] Zhang J, Lian L X, Liu Y and Wang R Q 2021 *Int. J. of Heat and Mass Trans.* **164** 120536.
[10] Deng D, Liang D, Tang Y, Peng J, Han X and Pan M. 2013 *Exp. Therm. and Fluid Sci*. **50** 1-9.
[11] Masoodi R, Pillai K M and Varanasi P P 2007 *AIChE Journal*, **53** 11, 2769-82.
[12] Deng D, Tang Y, Huang G, Lu L and Yuan D 2013 *Int. J. of Heat and Mass Trans*. **56** 1-2, 283-293.
[13] Eshghinejadfard A, Daróczy L, Janiga G and Thévenin D 2016 *Int. J. of Heat and Fluid Flow* **62** 93-103.
[14] Narváez A, Zauner T, Raischel F, Hilfer R and Harting J 2010 *J. of Stat. Mech.: Theory and Exp.* **2010** 11, P11026.
[15] Jeon S and Byon C 2017 *Int. J. of Heat and Mass Trans*. **115** 879-85.
[16] Otaru A J and Samuel M B 2021 *Mat. Res. Express* **8** 046516, 1-15.
[17] Jafari D, Wits W W and Geurts B J 2018 *App. Therm. Eng.* **143** 403–14
[18] Elkholy A, Durfee J, Mooney J P, Robinson A J and Kempers R 2023 *Meas. Sci. Technol*. **34** 045301
[19] OpenFOAM and The OpenFOAM Foundation, https://openfoam.org. Last access: April 2023.
[20] Guilizzoni M, Santini M, Lorenzi M, Knisel V and Fest-Santini S 2014 *J. of Phys: Conf. Series* **547** 012028
[21] Latt J, Malaspinas O, Kontaxakis D, Parmigiani A, Lagrava A, Brogi F, Ben Belgacem M, Thorimbert T, Leclaire S, Li S, Marson F, Lemus J, Kotsalos C, Conradin R, Coreixas C, Petkantchin R, Raynaud F, Beny J and Chopard B 2021 Palabos: Parallel Lattice Boltzmann Solver. In *Computers & Mathematics with Applications* **81** 334-350
[22] Gotoh R, Furst B I, Roberts S N, Cappucci S, Daimaru T, Sunada E T 2022. *Prog. Addit. Manuf.* **7**(5), 943–55.